TU Delft

Challenging Glass 3 – Conference on Architectural and Structural Applications of Glass, Bos, Louter, Nijsse, Veer (Eds.), TU Delft, June 2012.

The Mechanical Performance of Adhesives for a Steel-Glass Composite Façade System

Shelton Nhamoinesu, Mauro Overend
University of Cambridge, UK, sn393@cam.ac.uk , mo318@cam.ac.uk

High strength adhesives provide potentially efficient load-bearing steel-glass linear connections by enabling composite action. However, there is a lack of reliable models that can accurately predict their mechanical behavior. This paper describes experimental investigations undertaken to select suitable adhesives from short-listed epoxies and acrylates. The selection was based on mechanical performance of adhesive single-lap shear joints subjected to short-duration loads. The paper also assesses the validity of an analytical and a viscoelastic-plastic numerical model used for predicting the stress-state in adhesive joints. The investigation shows that three of the tested adhesives may be suitable for use in a steel-glass composite façade system. The analytical model provides good predictions at low strains but the accuracy decreases with increasing adhesive strains. The non-linear numerical model provides reasonable predictions but is sensitive to adhesive shear modulus history.

Keywords: Structural Adhesives, Steel-Glass Composite Façade System, Single-Lap Shear (SLS) Test

1. Introduction

Despite the ubiquity of bolted connections in structural glazing systems, adhesive connections are gaining popularity. Unlike bolted connections that weaken the glass in the vicinity of bolt holes, adhesive bonding ensures a more uniform load transfer between glass and the supporting elements. As a result, efficient composite behaviour between glass and the supporting elements can be achieved.

Studies aimed at understanding the mechanical behaviour of adhesive joints date back to the mid-1940s when Goland and Reissner '[1]' proposed an empirical moment distribution approach for determining the stress-state in a lap joint. They derived expressions for the distribution of shear stress across an adhesive in a lap-shear joint with similar adherends. More recently, Bigwood and Crocombe '[2]' proposed a general elastic analysis where adherends act as cylindrically bent plates connected along adjacent interfaces by an adhesive layer capable of transmitting both shear and tensile loads. Their approach is an extension of Goland and Reissner's empirical moment distribution but has been extended to analyse dissimilar adherends.

There are many adhesives produced by different manufacturers which can be potentially used for steel to glass connections. Perhaps the best known are the structural silicone sealants which are increasingly being used to achieve flexible structural connections between glass and aluminium or steel or between glass and glass. Compared to other types of adhesives, silicones are better understood in terms of their mechanical performance and durability. These are well documented in several standards and codes such as BS 6262-6: 2005 '[3]', EOTA 1988 '[4]', AAMA CW-13-85 '[5]' and ASTM C

1401-02 '[6]'. Structural silicone joints are relatively thick and flexible, thereby allowing them to accommodate differential thermal strains between glass and metallic sub-frames. However with tensile strengths of only 0.8 to 1.8MPa '[7]' for dynamic loading, structural silicones are unsuitable for transferring the higher longitudinal shear required for composite action in a typical steel-glass composite façade system.

Several studies on high strength thermosetting adhesives '[8], [9], [10], [11], [12], [13], [14]' have shown that there is a possibility of using stiffer adhesives such as epoxies and acrylates for bonding metal to glass. There is however a lack of confidence in the use of such adhesives for structural applications partly because of a lack of reliable models that can accurately predict their transient and long-term mechanical behaviour.

Significant research has been done to select the most suitable adhesives for metal to glass connections '[13]' and '[14]'; this paper caries forward the selection process by adapting a selection criterion that is specific for a typical steel-glass composite façade system. Six candidate adhesives were investigated:

- Two of the adhesives, the 3M two-part epoxy DP490 and the Huntsman two-part acrylate Araldite 2047 were chosen on the basis of previous research by '[13]'.
- The other two adhesives, 3M two-part epoxy 2216B/A and the Holdtite two-part acrylate 3295 were chosen on the basis of research done by '[14]'.
- The fifth adhesive, 3M two-part epoxy/acrylate hybrid 7271 B/A is a new product on the market that was recommended by the manufacturer as a potential metal to glass adhesive.
- The sixth adhesive, Dow Corning two-part silicone DC993 was chosen as a control adhesive since its material properties are well documented in the Dow Corning product data sheet '[15]' and its mechanical behaviour has been extensively investigated '[13], [14], [16]'.

This paper firstly outlines the determination of bulk material properties of the six candidate adhesives by uniaxial tensile tests on dumbbell specimens. The material properties were implemented into an analytical model '[2]' as well as into a commercially available finite element analysis (FEA) software, LUSAS v14.3 '[17]'. The FEA analyses utilized a viscoelastic-plastic constitutive model as well as a simple linear elastic perfectly plastic constitutive model. The models were used to predict the mechanical performance of specially adapted steel-glass single-lap shear (SLS) joints. Validation of the models was done experimentally by steel-glass SLS tests based on ASTM D1002-99 '[18]'. Whilst different adhesives perform optimally at different bond thicknesses, all the specimens in this investigation were prepared with a bond thickness of 3mm which is the minimum gap-fill governed by the fitness tolerances in the end-application. In addition to performing the tests at ambient temperature, specimens previously exposed to 80^0C for *48hrs* were also tested to investigate the effect of extreme temperature on joint performance.

Finally, the results of the SLS tests and the validity of the analytical and numerical models were discussed. The selection criterion for the adhesives most suitable for the steel-glass composite façade system was as follows:

- cohesive or adherend failure preceded by substantial plastic strain in the adhesive
- relatively high joint flexibility
- adhesive shear strength of at least *7.5MPa*
- minimum loss of strength after exposure to temperatures of up to 80^0C

2. Analytical and Numerical Predictions

2.1. Experimental Determination of Material Properties

4mm thick dumbbells of the six candidate adhesives, sized to comply with '[19], [20]' (Fig.1a) were prepared by casting the adhesives into an aluminium cut-out mould lined by a PTFE release film (Fig.1b). Air bubbles caused by the chemical reaction of the adhesive components were minimized by placing the cast mould into a vacuum chamber; the aluminium mould also acted as a heat sink that reduced bubble formation. Two different uniaxial tensile tests were performed on each of the adhesives in order to determine the following bulk material properties: (i) visco-elastic shear modulus G_v, (ii) visco-elastic decay constant β, (iii) elasto-plastic stress-strain relationship and (iv) poisson's ratio υ.

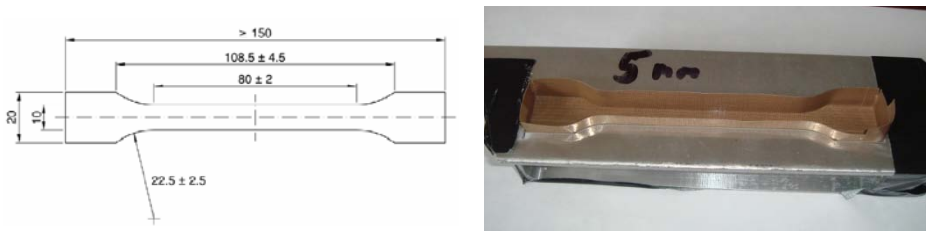

Figure 1: (a) Dumbbell geometry '[18],[19]' and (b) PTFE lined aluminium mould

The first test was performed to determine the visco-elastic properties G_v and β. An instantaneous tensile load was applied to the dumbbells at a high extension rate of *100mm/min* up to an extension of *1mm* followed by strain holding for approximately *500s* while recording the decaying stress. The stress-time curve was converted into a shear modulus-time curve (Fig.2a); β was determined by curve fitting of Eq.1. G_v was obtained by subtracting the residual shear modulus G_∞ from the initial shear modulus G_0.

$$G(t) = G_v e^{-\beta t} = \left(G_0 - G_\infty\right) e^{-\beta t} \tag{1}$$

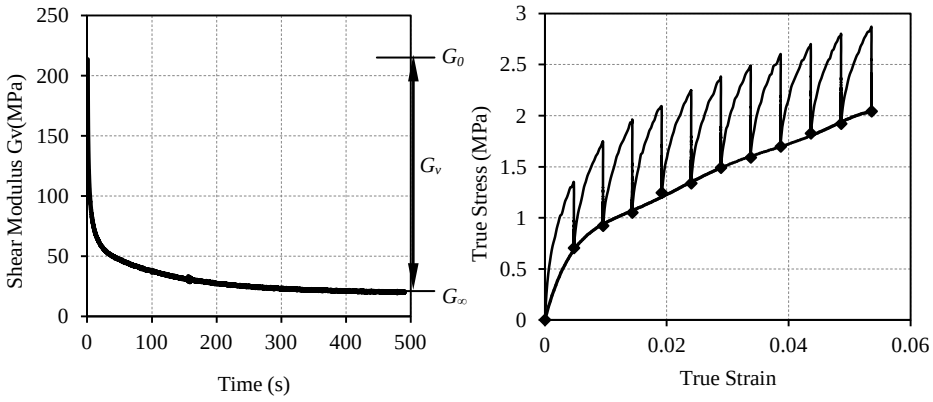

Figure 2: (a) Shear modulus *vs.* time and (b) True stress/relaxation *vs.* true strain curves for 3M 2216 B/A epoxy dumbbell. The dotted curve is the time-independent true stress *vs.* true strain

The second test was performed to determine the elasto-plastic properties of the adhesives by adopting a discrete load-step strategy on the dumbbell specimens '[14]'. The total loading period was divided into approximately ten intervals and at each interval; the strain was increased by *0.005* followed by strain holding for a period equal to the decay time t_d from Figure 2a above. A time-independent elasto-plastic relationship was obtained by curve fitting of the discrete points on the true stress *vs.* true strain graph (Fig.2b). The experimentally obtained material properties of the candidate adhesives are summarised in Table 1 below.

Table 1: Material properties of the six candidate adhesives

	Poisson's Ratio ν	Shear Modulus G_v (MPa)	Elastic Modulus E_0 (MPa)	Decay Constant β	Time independent elasto-plastic stress-strain polynomial
3M DP490 Epoxy	0.38	239.0	659.6	0.001	$\sigma = -27568\varepsilon^2 + 1305.1\varepsilon + 0.0013 \quad \varepsilon \leq 0.014$ $\sigma = -6552.7\varepsilon^2 + 684.03\varepsilon + 4.4918 \quad \varepsilon > 0.014$
Araldite 2047 Acrylice	0.43	211.0	603.5	0.002	$\sigma = -16881\varepsilon^2 + 766.43\varepsilon + 0.1549 \quad \varepsilon \leq 0.025$ $\sigma = -1300.5\varepsilon^2 + 141.34\varepsilon + 6.3631 \quad \varepsilon > 0.025$
3M 7271 Epxy/Acylic	0.29	559.0	1142.2	0.003	$\sigma = -35361\varepsilon^2 + 1283.5\varepsilon \quad \varepsilon \leq 0.01$ $\sigma = -18645\varepsilon^2 + 945.9\varepsilon + 1.7463 \quad \varepsilon > 0.01$
3M 2216 B/A Epoxy	0.47	192.4	565.6	0.007	$\sigma = -10755\varepsilon^2 + 199.14\varepsilon \quad \varepsilon \leq 0.01$ $\sigma = -133.73\varepsilon^2 + 33.495\varepsilon + 0.6172 \quad \varepsilon > 0.01$
Holdtite 3295 Acrylate	0.41	219.5	619.0	0.002	$\sigma = -12430\varepsilon^2 + 525.25\varepsilon - 0.0061 \quad \varepsilon \leq 0.015$ $\sigma = -886.79\varepsilon^2 + 147.7\varepsilon + 3.009 \quad \varepsilon > 0.015$
DC 993 Silicone	0.48	3.9	11.5	0.004	$\sigma = -17.612\varepsilon^4 + 22.002\varepsilon^3 - 10.069\varepsilon^2$ $+2.351\varepsilon + 0.0003$

2.2. Analytical Model

Using material data from Table 1 above, stresses across the adhesive layer in a lap-shear joint (Fig.3) can be predicted by the Crocombe and Bigwood linear elastic analytical model'[2]'. The model is based on a seventh order differential equation (Eq.2) and a sixth order differential equation (Eq.3) that describes the shear stress τ_{xy} and the transverse stress σ_y distributed across the adhesive layer of a lap shear joint.

$$\frac{d^7\tau_{xy}}{dx^7} - K_1\frac{d^5\tau_{xy}}{dx^5} + K_3\frac{d^3\tau_{xy}}{dx^3} - K_5\frac{d\tau_{xy}}{dx} = 0 \tag{2}$$

$$\frac{d^6\sigma_y}{dx^6} - K_1\frac{d^4\sigma_y}{dx^4} + K_3\frac{d^2\sigma_y}{dx^2} - K_5\sigma_y = 0 \tag{3}$$

where K_1 to K_5 are constants dependent on the shear modulus of the adhesive and the elastic moduli of the adherends.

Crocombe and Bigwood created a spreadsheet that solves equations 2 and 3 if the applied loads (P_1, P_2, V_1, V_2, M_1 and M_2) shown in Figure 3 above are known. The determination of the bending moments M_1 and M_2 is relatively complex, in this paper, values of M_1 and M_2 were obtained using an analytical derivation presented in '[21]'. The graphical presentation of the Crocombe and Bigwood elastic stress distribution across the *30mm* length of the SLS joint of each candidate adhesive is shown in Figure 4 below. The stress distributions in Figure 4 correspond to the six mean failure loads *P* obtained from SLS experimental tests of each candidate adhesive.

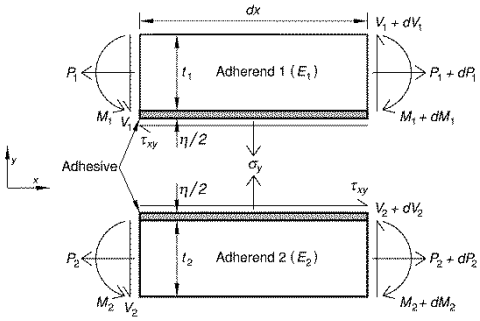

Figure 3: Free-body diagram of element *dx* along single-lap adhesive joint '[2]'

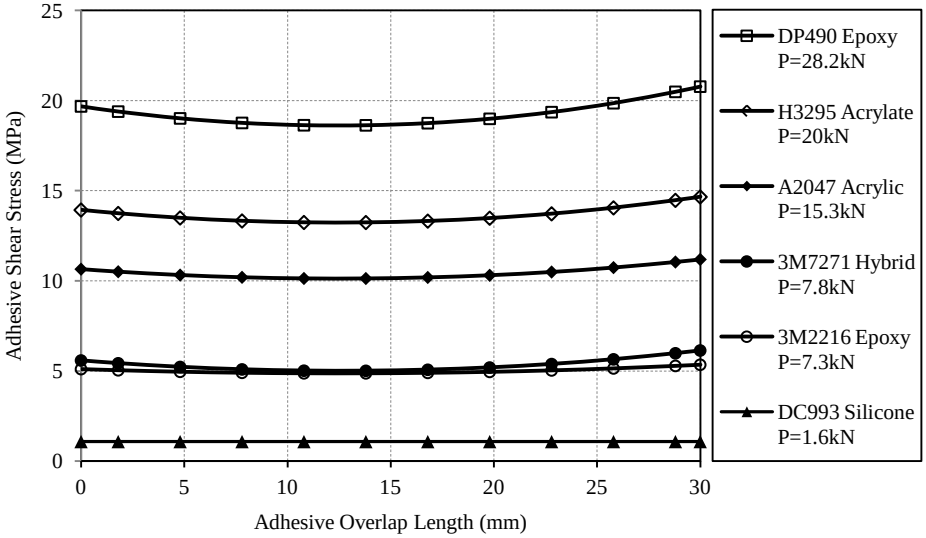

Figure 4: Bigwood and Crocombe shear stress distribution plots across SLS adhesive joints

2.3. Numerical Model

The steel-glass SLS test was constructed as a 2-dimensional FEA model using LUSAS *v*14.3 '[17]'. An eight node quadrilateral quadratic plane strain element type was implemented throughout the model. Since the SLS joint is symmetrical about the midpoint of the glass (line *y-y* in Fig.5), only half of the connection is modeled.

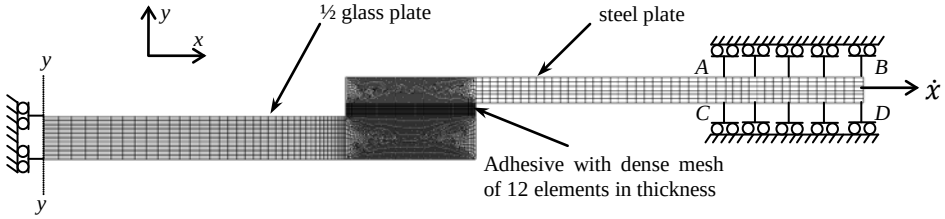

Figure 5: Two dimensional FEA model of the steel-glass adhesive SLS connection.

For the boundary conditions, the model was restrained in δ_x and M_z along the symmetry line *y-y* and also restrained in δ_y and M_z along the lines *AB* and *CD* which represent the contact of the steel plate to the testing machine. The glass and steel were modeled as perfectly linear elastic materials with $E_{glass}=70GPa$, $v_{glass}=0.23$, $E_{steel}=209GPa$ and $v_{steel}=0.3$. The six candidate adhesives were modeled with visco-elastic and elasto-plastic properties obtained from Table 1. A velocity $\dot{x}$ was applied at the end of the steel plate, line *BD* and it corresponds to the experimental displacement rate of *0.2mm/min*. The analysis was run as a dynamic geometric and material non-linear analysis using the implicit method and an updated langrangian approach. The results of the numerical analysis were compared to the analytical and experimental test results in Section 4.
In addition to the non-linear analysis described above, a simple linear elastic analysis was performed. The adhesives were modeled with linear elastic-perfectly plastic material properties obtained from the time-independent elasto-plastic stress-strain plots (Fig.2b).

3. Steel-Glass Single-Lap Shear Joint Tests

3.1. Specimen Preparation

Specially adapted SLS adhesive joints (Fig.6a,b) of the six candidate adhesives were prepared based on ASTM D1002-99 '[18]' guidelines. Each specimen was assembled using two *120mm* by *49mm* by *6mm* thick black mild steel plates and one *200mm* by *200mm* by *10mm* thick fully toughened glass plate manufactured to BS EN12150-2 '[22]' standards. The bonding surface of the steel was sanded using a *220* grit sandpaper to give a consistent finish for all specimens. All steel and glass surfaces were thoroughly cleaned with acetone before adhesive application and in the case of the silicone joints; a siloxane based primer was applied to the steel surface before bonding the adherends. A specially machined aluminium jig lined with a PTFE release film was used for assembling all specimens; the jig ensured alignment of the two steel plates as well as maintaining a bond thickness of *3mm* for all specimens. All joints had a bond width of *49mm* and a bond length of *30mm*. All the six candidate adhesives were two-part pot adhesives and mixing conformed to each of the manufacturer's guidelines. The prepared specimens were stored at ambient temperature and approximately *40%* relative humidity.

3.2. Test Procedure

The SLS tests were performed on an Instron 5500R testing machine with a *150kN* load cell. Specimens were attached to the testing machine by slotting steel pins into *12mm* holes which are *20mm* from the end of each steel plate. A displacement gauge was attached to each steel plate with the gauge probe resting on an aluminium plate glued to the centre of the glass plate (Fig.6b). The displacement gauges separately measured the vertical displacement in each adhesive joint. All tests were displacement controlled and a displacement rate of *0.2mm/min* was applied for all specimens except for the very flexible silicone DC993 specimens which were tested at *1.0mm/min*. Photographs were taken before, during and after each test. The tests were divided into two phases.
Phase 1: Three specimens of each of the six candidate adhesives were tested at 21^0C.
Phase 2: Three specimens of the best-performing adhesives from Phase 1 were heat-soaked in an oven at 80^0C for *48hrs* and then tested at 21^0C.

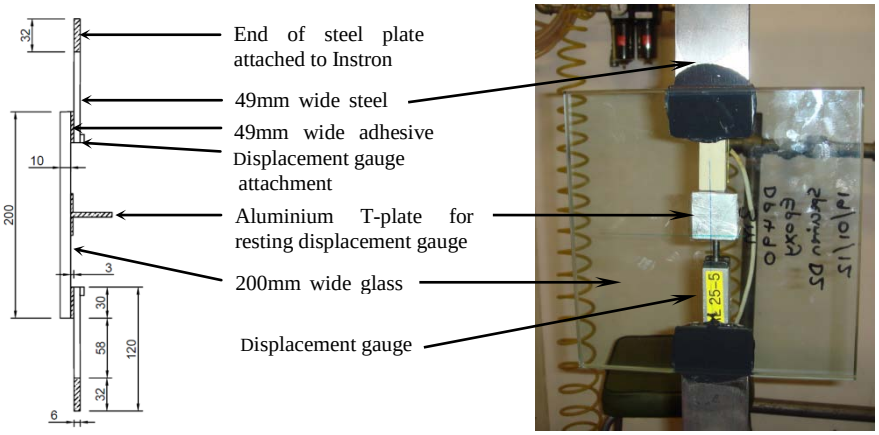

Figure 6: (a) Schematic drawing and (b) photograph of the SLS test set up

3.3. Test Results

Phase 1: All DC993 silicone specimens failed cohesively with very low failure loads but large extensions. Although the failure mode is desirable and the adhesive showed remarkable flexibility, the calculated mean shear strength of only *1.1MPa* makes the silicone unsuitable for the steel-glass composite system being developed. All 3M DP490 epoxy joints experienced glass failure preceded by brittle partial failure in the adhesive. There was no plastic deformation observed (Fig.7) and the DP490 joints experienced the highest failure loads of up to *28kN*. The lack of flexibility and lack of plastic deformation before failure makes DP490 unsuitable. The 3M 7271 epoxy/acrylate hybrid joints experienced very small strains before failure. Glass failure at relatively low loads and very low extensions was observed in all specimens. Holdtite 3295 acrylate specimens carried significantly high loads and were relatively flexible. The adhesive exhibited considerable plastic deformation (Fig.7) before local glass failure on the glued glass edges. The 3M 2216 epoxy specimens showed good flexibility but the load carrying capacity was relatively low with maximum loads of only *7.3kN*. Adhesion failure at the steel-adhesive interface was observed in all 3M 2216 specimens, this seemed to suggest premature joint failure. This observation could be attributed to potential inadequate surface preparation or to large bond thickness since previous studies '[14]' have shown that this epoxy predominantly fails cohesively. The Araldite A2047 acrylate showed the best results. All specimens failed cohesively after substantial plastic deformation. The joints were relatively more flexible yet they carried significantly high loads of up to *15.3kN*.

Phase 2: The 3M 2216 epoxy, Araldite A2047 and Holdtite 3295 acrylate adhesives were also tested after heat soaking at 80^0C for *48hrs*. The 3M 2216 joints performed poorly; failing to carry loads above *1kN*. As in phase 1, inadequate surface preparation may be the cause of premature failure. The Araldite A2047 joints showed good strength after heat soaking with only about *18%* strength reduction (Fig.7). Failure was still cohesive with substantial plastic deformation in the adhesive occurring prior to failure. Holdtite 3295 joints performed very well after heat soaking, with a typical strength reduction of only *13%* (Fig.7). Glass failure occurred and was preceded by substantial plastic deformation in the adhesive. Table 2 below summarises the test results.

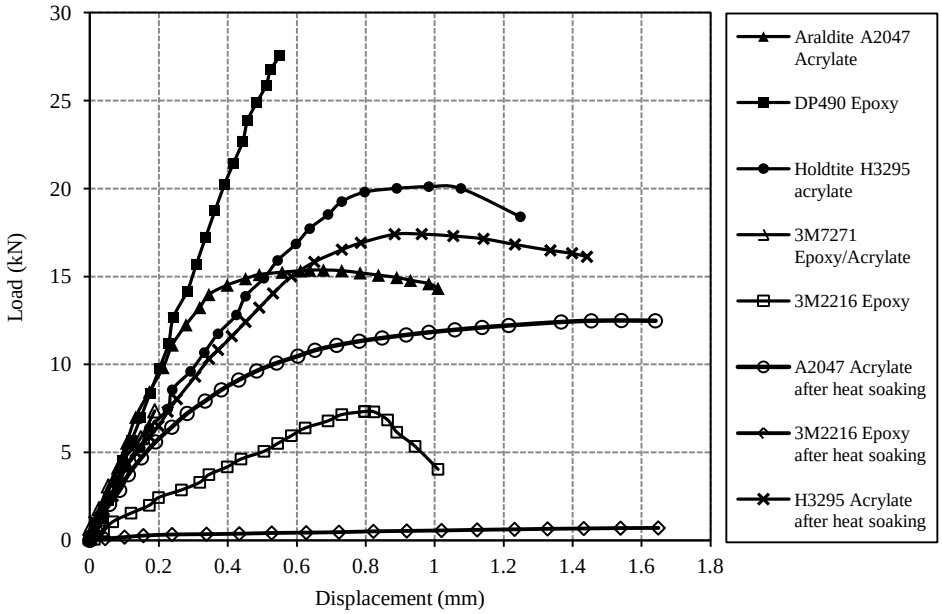

Figure 7: Typical SLS test load vs. extension curves for five candidate adhesives (DC993 Silicone is excluded for clarity)

Table 2: Summary of experimental results

	Mean Failure Load (kN)	Extension at failure (mm)	Mean Shear Strength [a] (MPa)	Mode of failure
3M DP490 Epoxy	28.2	0.56	19.2 [b]	Glass failure, no plastic strain in the adhesive prior to failure
Araldite 2047 Acrylic	15.3 (12.5[*])	1.04 (1.28[*])	10.4 (8.5[*])	Cohesive failure preceded by substantial adhesive plastic strain
3M 7271 Epxy/Acylic	7.8	0.20	5.3 [b]	Glass failure, no plastic strain in the adhesive prior to failure
3M 2216 B/A Epoxy	7.3 (0.7[*])	0.85 (1.71[*])	5.0 (0.5[*])	Adhesion failure at the steel-adhesive interface
Holdtite 3295 Acrylic	20.0 (17.4[*])	1.25 (1.44[*])	13.6[b] (11.6[*])[b]	Glass failure preceded by significant adhesive plastic strain
DC 993 Silicone	1.6	5.61	1.1	Cohesive failure preceded by high adhesive plastic strain

[*] specimens subjected to 80^0C for 48hrs before testing
[a] based on equivalent constant shear stress along the lap joint and loading is short term
[b] adhesive shear strength governed by glass failure

4. Discussion

Comparison of the linear elastic analytical Bigwood and Crocombe model to both linear elastic and non-linear viscoelastic-plastic FEA models (Fig.8) generally reveal that there is good agreement particularly for small loads. This is not surprising since the linear-elastic analytical model by definition should predict the elastic deformation which is predominant at small strains. As the failure load is approached and strains become larger, the analytical model tends to underestimate the adhesive shear stress (Fig.8) by magnitudes of up to 16.7%. This is uncharacteristic since elastic stresses are expected to be larger than elasto-plastic stresses. Unlike the linear elastic FEA model, the non-linear FEA model does not show prominent stress peaks near the joint edges at high loads, this is due to prediction of plasticity in the non-linear model.

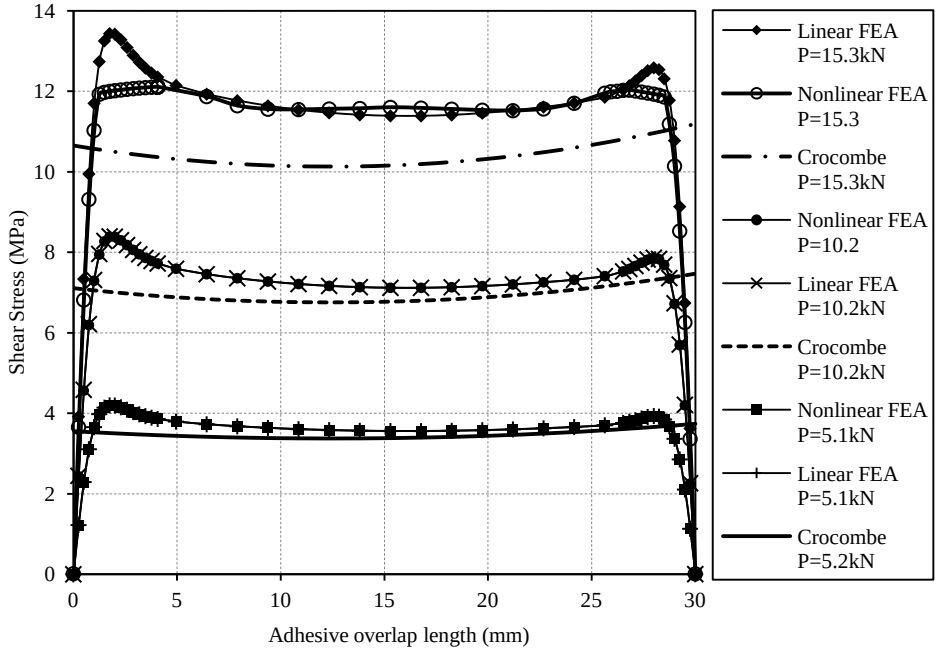

Figure 8: Analytical and numerical shear stress distribution across the Araldite A2047 acrylate SLS adhesive joint

Despite the limitations of the analytical model, experimental mean shear strengths of the adhesives (Table.2) show very good agreement with the Bigwood and Crocombe's predictions of adhesive shear stress at failure load (Fig.4).

For most of the candidate adhesives, numerical results for load *vs.* extension generally showed good agreement at low strains (Fig.9). As strains in the SLS joint increased, numerical models showed varying degrees of accuracy for different adhesives. The accuracy of the non-linear model seemed to heavily depend on the value of the decay constant β. Mathematical analysis of experimentally obtained shear modulus *vs.* time

plots suggested that the shear modulus history of the tested adhesives *G(t)* is best described by a logarithmic function (Eq.4) below.

$$G(t) = -\alpha \ln(t) + \gamma \tag{4}$$

where α and γ are constants. However the FEA constitutive model used in this study describes *G(t)* by an exponential function (Eq.1). As a result, an estimation of β was required to allow Eq.1 to approximate Eq.4 and this invariably limited the accuracy of the constitutive model.

The predictive capability of the models is also dependent on the adhesive failure mode; lap shear joints that experience adhesion or glass failure tend to be predicted poorly compared to those that fail cohesively. In the case of the 3M 2216 Epoxy adhesive joints, for example, where failure was by adhesion at the steel-adhesive interface, the numerical predictions were unsatisfactory.

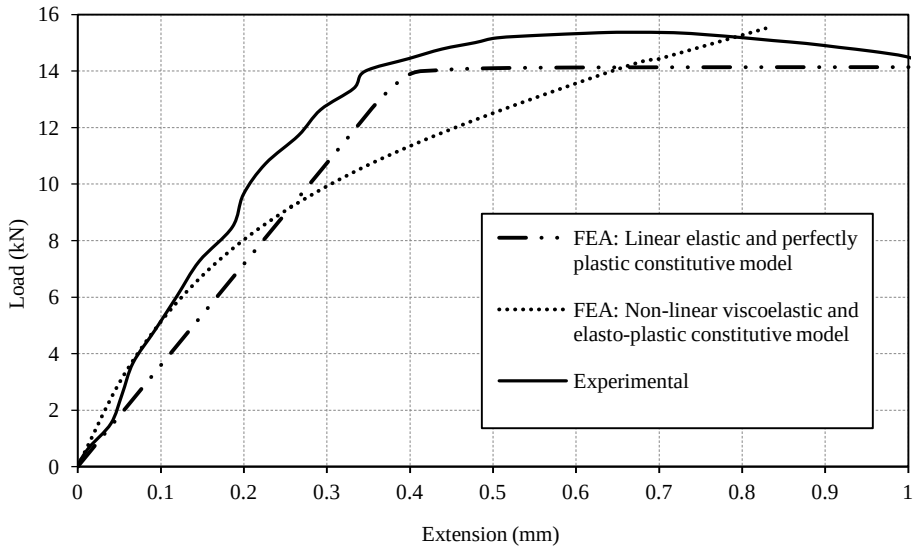

Figure 9: Experimental and numerical load *vs.* extension plots for Araldite A2047 acrylate SLS adhesive joint

5. Conclusion

The main objective of this paper was to identify suitable structural adhesives for a steel-glass linearly bonded system. SLS tests on the six candidate adhesives provided significant information which indicated that at least three of the six adhesives may be suitable for the proposed system.

Out of all the tested adhesives, it was concluded that the Araldite A2047 acrylate SLS joints exhibit the most desirable mechanical characteristics under short-duration testing conditions. The Araldite A2047 acrylate SLS joint:

- failed cohesively both in specimens tested before and after heat soaking at 80^0C for *48hrs*

- showed good strength with mean shear strength of *10.4MPa*
- exhibited relatively good flexibility with substantial plastic deformation preceding failure
- was not significantly affected by exposure to extreme temperature, with a maximum percentage drop in load bearing capacity of only *18%*
- was relatively easy to prepare and handle.

Holdtite 3295 acrylate also performed well, the mean shear strength of *13.6MPa* was based on glass failure therefore it is likely that the adhesive is even stronger than this. The Holdtite adhesive was relatively flexible and it experienced considerable plastic strain before local glass failure, this was especially evident in specimens tested after heat soaking. The Holdtite 3295 also had the best strength retention after heat soaking with only 13% reduction in load bearing capacity. However, when compared to Araldite A2047, the Holdtite 3295 joints were more difficult to prepare owing to the low viscosity and short curing time. Although the 3M 2216 Epoxy showed poor adhesion to the metal surface; its relatively good flexibility, significantly good strength, low cost and relatively long handling time warrants its consideration for further investigation. The other three adhesives were found to be unsuitable for different reasons ranging from significantly low strength in the case of DC993 silicone to significant lack of flexibility in the case of DP490 epoxy and 3M 7271 epoxy/acrylate hybrid. It must be noted however that the elimination of some of these adhesives did not necessarily mean they are not suitable for steel to glass connection; this study presented a specific bond line thickness of 3mm, a constraint which limits the performance of some adhesives which are otherwise suitable for bonding steel to glass.

The other objective of this paper was to validate the predictive capability of an analytical model and a viscoelastic-plastic numerical model. It was shown that the linear-elastic analytical model is useful in predicting adhesive joint behaviour at low strains but the accuracy decreases as the adhesives start to experience plastic deformation at large strains. It was also shown that the non-linear numerical model provides reasonable predictions of stress distribution across adhesive joints but requires good approximation of the adhesive shear modulus history function *G(t)*. Research aimed at improving the adhesive constitutive model by accounting for effects of hysteresis and repeated cyclic loading is underway and results are due to be published in the near future. It is hoped that these improved models can be used to predict the global adhesive joint performance in full-scale steel-glass composite façade modules.

6. Acknowledgements

The study presented in this paper, which forms part of a broader ongoing research aimed at developing a steel-glass composite façade system is funded by an Industrial CASE studentship provided by the Engineering and Physical Sciences Research Council (EPSRC) and a contribution from TATA Steel, the Industrial partner.

7. References

[1] Goland, M; Reissner, E, *The stresses in cemented joints*, J Appl Mech Trans ASME **66** (1944), Vol.11, ppA17-A27.

[2] Bigwood, D.A; Crocombe, A.D, *Elastic analysis and engineering design formulae for bonded joints*, Int J Adhes Adhes (1989), Vol.9, No.4, pp229-242.

[3] BS 6262-6: 2005, *Code of practice for glazing for buildings – Part 6: Code of practice for special applications*, British Standards Institution BSI (October 2005).

[4] ATAG Nr 002, European Organisation for technical Approvals EOTA, Brussels (1998).

[5] AAMA CW-13-85, *Structural sealant glazing systems*, American Architectural Manufacturers Association (AAMA), Schaumburg, USA (1985).

[6] ASTM C 1401-02, *Standard guide for structural sealant glazing*, ASTM Standards (2002).

[7] Haldimann, M; Luible, A; Overend, M, *Structural use of glass*, Structural Engineering Documents SED10, International Association for Bridge and Structural Engineering IABSE, Zurich, May 2008.

[8] Močibob, D; Crisinel, M, *Linear connection system for structural application of glass panels in fully-transparent pavilions*, Proceedings of Challenging Glass 1, Delft, Netherlands, 2008.

[9] Pye, A; Ledbetter, A, *The selection of an adhesive for a glass-adhesive T-beam*, Int J Adhes Adhes (1998), Vol 18, pp159-165.

[10] Wellershoff, F; Sedlacek, G, *Glued connections for new steel glass structures*, Proceedings of Glass Performance Days, Tampere, Finland, 2005.

[11] Louter, C; Veer, F; Hobbelman, G, *reinforcing glass, effects of reinforcement geometry and bonding technology*, Proceedings of Glass Performance Days, Tampere, Finland, 2007.

[12] Weller, B; Schadow, T, *Design of bonded joints in glass strucutres*, Proceedings of Glass Performance Days, Tampere, Finland, 2007.

[13] Belis, J; Van Hulle, A; Out, B; Bos, F; Callewaert, D; Poulis, H, *Broad screening of adhesives for glass-metal bonds*, Proceedings of Glass Performance Days, Tampere, Finland, 2011.

[14] Overend, M; Jin, Q; Watson, J, *The Selection and Performance of Adhesives for a Steel-Glass Connection*, Int J Adhes Adhes (2011), doi:10.1016/j.ijadhadh.2011.06.001.

[15] DC993 Product Data Sheet, http://www.geocel.co.uk/dynpdfs/416.pdf, http://www.dowcorning.com/, Ref No. 62-0918H-01, Dow Corning Corporation, July 2001.

[16] Močibob, D, *Glass panel under shear loading – use of glass envelopes for building stabilisation*, PhD Thesis, Swiss Federal Institute of Technology (EPFL), Lausanne, Switzerland, 2008.

[17] LUSAS Finite Element System, *Lusas theory manual*, FEA Ltd, UK, (2012).

[18] ASTM D 1002-99, *Standard test method for apparent shear strength of single-lap-joint adhesively bonded metal specimens by tension loading (Metal-to-metal)*, ASTM Standards (1999).

[19] BS EN ISO 527-1: 1996, *Plastics – Determination of tensile properties – Part 1: General principles*, pp. 1-16, British Standards Institution BSI (1996).

[20] BS EN ISO 527-2: 1996, *Plastics – Determination of tensile properties – Part 2: Test conditions for moulding and extrusion plastics*, pp. 1-14, British Standards Institution BSI (1996).

[21] Cheng, S; Chen, D; Shi, Y, *Analysis of adhesive-bonded joints with non-identical adherends*, J Engineering Mechanics (1991), Vol.117, No.3.

[22] BS EN ISO 12150-2: 2004, *Glass in buildings: Thermally toughened soda-lime silicate safety glass, evaluation of conformity/product standard*, pp. 1-42, British Standards Institution BSI (2004).